Density-Induced Phase Separation in Poly(ethylene-*co*-1-butene)−Dimethyl Ether Solutions

D. Li,[†] M. A. McHugh,*[,†] and J. H. van Zanten*[,‡]

Department of Chemical Engineering, Virginia Commonwealth University, Richmond, Virginia 23284, and Department of Chemical and Biomolecular Engineering, North Carolina State University, Raleigh, North Carolina 27695-7905

Received September 7, 2004; Revised Manuscript Received December 24, 2004

ABSTRACT: Dynamic light scattering measurements are reported for poly(ethylene-*co*-20.2 mol % 1-butene) (PEB_{10}) in dimethyl ether (DME) at 110−170 °C and pressures to 2500 bar. The cloud-point curve for the PEB_{10}−DME system exhibits both low- and high-pressure upper consolute solution temperature (UCST) branches. The polymer infinite dilution translational diffusion coefficient, D_0, increases with increasing temperature and decreasing pressure as expected. The observed variation of D_0 is inversely proportional to the solvent viscosity, indicating that the polymer coil hydrodynamic size is independent of temperature and pressure. The dynamic second virial coefficient, k_D, which represents a balance between thermodynamic interactions and hydrodynamic forces, displays values that lie within the bounds expected for Θ and good solvent conditions. While the low-pressure UCST is classical in that the polymer−solvent interactions become unfavorable upon approach to this phase boundary, the high-pressure UCST branch exhibits anomalous behavior wherein polymer−solvent interactions improve as this phase boundary is approached. Such behavior suggests that the phase separation is entropic in origin and is driven by unfavorable mixing effects.

Introduction

The study of polymer−polymer interactions in dilute solution dates back to Flory, Zimm, and other investigators working a half century ago. These studies elucidated the role played by temperature in modulating polymer−polymer interactions, thereby leading to the development of the excluded-volume concept.[1] Static light scattering measurements, along with viscometry and osmotic pressure methods, yielded extensive information on the polymer radius of gyration, R_g (i.e., chain dimension), as well as the second osmotic virial coefficient, A_2, for a large number of polymer−solvent pairs. The development of dynamic light scattering (DLS) methods[2,3] ultimately allowed for the determination of analogous dynamical quantities—the hydrodynamic radius, R_H, and dynamic second virial coefficient, k_D—which accounts for both thermodynamic and hydrodynamic interactions. Akcasu and co-workers developed a method for incorporating both static and dynamic light scattering measurements into a detailed picture of polymer−polymer interactions in solution.[4−6] Cotts and Selser subsequently provided a particularly illustrative exposition of these ideas with a detailed exploration of molecular weight effects on polymer−polymer interactions.[7]

Although scattering methods have been extensively used to investigate polymer−polymer interactions in solution, these earlier studies primarily utilized incompressible liquid solvents at ambient pressures and the application of temperature to modulate solvent quality. In contrast, the effect of pressure on polymer solution microstructure has received little consideration, especially for solutions with compressible gases as the solvent of interest. Lechner and co-workers reported high-pressure light scattering studies for polymer−liquid solvent systems that date to the early 1970s.[8−12] Dynamic light scattering was used to show that the polymer diffusion coefficient at infinite dilution, D_0, increases with increasing temperature but is relatively insensitive to pressure, except at high temperatures.[11,12] In addition, the changes in D_0 were directly related to the increase of solvent viscosity with pressure, which suggests that polymer−liquid solvent systems at high pressure are reasonably well understood. These early observations as to the primacy of pressure-driven viscosity effects have also been confirmed in the polystyrene−toluene system by others including the current investigators most recently.[13−15] In the early 1970s, Gaeckle and Patterson performed static light scattering studies with solutions of poly(isobutylene) (PIB) in 2-methylbutane and poly(styrene) (PS) in 2-butanone.[16] They showed that pressure has a strong effect on polymer−solvent interactions, which results in a ∼10% increase in R_g for the PIB−2-methylbutane solution and a ∼5% increase in R_g for the PS−butanone solution. The second osmotic virial coefficient, A_2, also increased from a small negative value at pressures less than 50 bar to a small positive value at pressures ranging from 50 to 110 bar for PIB-2-methylbutane solutions at 57 and 64 °C.[16] A_2 did not significantly increase at 24 °C for the PIB−2-methylbutane system or at 22 °C for the PS−2-butanone system. Although this particular study considered pressures only up to 110 bar, the authors argued that pressure-induced density changes (i.e., packing effects) appreciably affect the polymer conformation or rotational isomer population. This interpretation is somewhat problematic since the solvent density only increases by ∼7% over this range of operating conditions, which are at modest temperatures and moderate pressures far from the solvent critical point. Sun and King demonstrated that polymer−solvent interactions

[†] Virginia Commonwealth University.
[‡] North Carolina State University.
* Corresponding authors: e-mail mmchugh@vcu.edu (M.A.M.) or john_vz@ncsu.edu (J.H.v.Z.).

10.1021/ma048166y CCC: $30.25 © 2005 American Chemical Society
Published on Web 02/22/2005

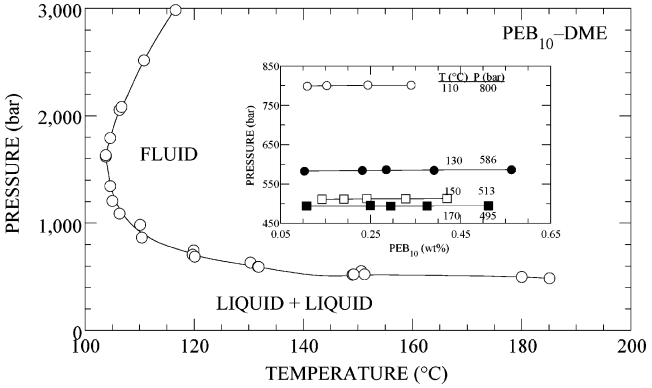

Figure 1. Phase behavior of a 5 wt % PEB_{10}–dimethyl ether (DME) solution. The inset graph shows the effect of concentration on the phase boundary of dilute PEB_{10}–DME solutions where the transition temperature and pressure are listed next to each curve.

steadily degrade and concomitantly influence polymer conformation upon approach to a pressure-induced, liquid–liquid phase boundary in aqueous poly(*N*-vinyl-2-pyrrolidone) (PVP) solutions.[17] PVP readily dissolves in water at ambient conditions but precipitates at pressures in excess of 3000 bar at room temperature. They propose that the increase in water density at high pressures disrupts PVP–water hydrogen bonding, which in turn induces phase separation. Recently, van Hook and co-workers generated a number of scattering studies exploring the role played by pressure in modulating polymer solution microstructure and, ultimately, macroscopic phase behavior.[18–23] They coupled DLS and small-angle neutron scattering (SANS) studies to probe the change of intermolecular and intramolecular correlation lengths over wide ranges of operating variables, but again, these studies were performed primarily with liquid solvent. More recently, Moses and van Hook demonstrated that the pressure sensitivity of A_2 depends on the proximity to the Θ point for a polymer–liquid solvent system.[24]

The objective of the present work is to relate the macroscopic phase behavior of PEB_{10}–DME mixtures to the solution microstructure and to polymer–polymer interactions in the single-phase region. This study is motivated by the interesting phase behavior of the PEB_{10}–DME system, which exhibits both low- and high-pressure upper consolute solution temperature (UCST) branches[25] (see Figure 1). The existence of these two branches has been corroborated with SANS measurements which indicate rapid growth of the solution correlation length near both boundaries indicative of incipient phase separation.[25] The DLS study is performed at 110, 130, 150, and 170 °C and at pressures close to the low-pressure UCST and increasing to 2500 bar into the single-phase region. At 110 °C DLS measurements probe the single-phase region near both the low-pressure and the high-pressure branches of the UCST. In contrast to operating with a liquid solvent, this DLS study is performed with DME, which is a highly compressible solvent in the pressure–temperature (P–T) region of interest, since these conditions are close to the critical temperature of DME (T_c = 126.8 °C) although the operating pressures are in excess of the DME's critical pressure (P_c = 52.4 bar). This coupled phase behavior–DLS study of nonpolar PEB_{10} in polar DME, which has a dipole moment of 1.3 D, complements an earlier study of PEB_{10}–nonpolar, compressible alkane solutions,[15] albeit with the addition of the high-pressure UCST branch in the current study.

Materials and Methods

Materials. The statistically random poly(ethylene-*co*-20.2 mol % 1-butene) (PEB_{10}, with 10 ethyl branches per 100 backbone carbon atoms; M_W of 232 500 and a M_W/M_N of 1.01–1.02) was synthesized by Pamela Wright and Lewis Fetters via anionic polymerization of butadiene with subsequent saturation by hydrogenation as described in detail elsewhere.[26–29] The PEB_{10} sample was stored at 5 °C and used without further purification. The dimethyl ether (99.8% purity, Aldrich Corp.) was used without further purification.

Dynamic Light Scattering. The high-pressure scattering cell is described in a previous report.[15] The system pressure is measured to within ±3.5 bar, and the solution temperature is maintained to within ±0.3 °C and is monitored with a thermocouple located directly in the solution. The incident radiation has a wavelength of 532 nm in vacuo (200 mW DPSS Nd:YAG, Coherent Inc.). A goniometer-mounted optical fiber transmits the collected scattered light to an ALV/SO-SIPD/DUAL photomultiplier detector (ALV-Laser). Autocorrelation functions are generated using an ALV-5000 multiple-tau digital correlator that operates in real time with a fixed range of logarithmically spaced lag times between 200 ns and several hours.

For homodyne DLS measurements, the normalized second-order intensity autocorrelation function, $g^{(2)}(q,\tau)$, can be related to the normalized first-order electric field autocorrelation function, $g^{(1)}(q,\tau)$:

$$g^{(2)}(q,\tau) = \beta|g^{(1)}(q,\tau)|^2 + B \tag{1}$$

where B is the baseline, τ is the lag time, and q is the scattering vector defined as $q = |q| = (4\pi n/\lambda_0)\sin(\theta/2)$, where θ is the scattering angle, λ_0 is the incident wavelength, and n is the solution refractive index. For the studies reported here the apparatus-dependent optical constant β is close to the ideal value of unity. The polymer cooperative translational diffusion coefficient, $D(c)$, is related to $\Gamma(q)$, the characteristic relaxation frequency of the system, which is taken to be the peak position of the spectra, $G(\Gamma)$, determined from eq 2 using a constrained regularization method.[30,31]

$$|g^{(1)}(q,\tau)| = \int G(\Gamma)e^{-\Gamma t}\,d\Gamma \tag{2}$$

It should be noted that a single-exponential fit to the correlation function or a cumulants analysis yields essentially the same Γ as the regularization method. As the high-pressure cell is much more difficult to clean than standard glass scattering cells, the authors prefer to use the regularization method to ensure that extraneous sources of scattering (i.e., dust contamination) are minimal. $D(c)$, calculated from a linear fit of $\Gamma(q)$ vs q^2, is assumed to represent the translational cooperative diffusion coefficient although the condition $qR_g \ll 1.0$ is not always satisfied for the systems considered here. The dilute solution refractive index is replaced with that of the pure solvent to determine q with little loss of accuracy. The Lorentz–Lorenz equation is used to account for the density dependence of the refractive index,[32–35] and the linearized Cauchy equation[36,37] is used to correct the refractive index for a λ_0 of 532 nm.

Density and Phase Behavior. The phase behavior for each PEB_{10}–DME mixture is determined using the scattering cell. The phase transitions, or cloud points, are the lowest operating pressure where the solution just begins to appear "hazy", the incident beam exhibits a halo due to multiple scattering, and the scattered light intensity increases substantially. DME density data shown in Figure 2 are also determined using a previously reported technique.[38–40] Specific experimental details of density measurement are given by Byun et al., who report that density measurements have an accumulated uncertainty of ±1.5%.[40] The mass density of DME

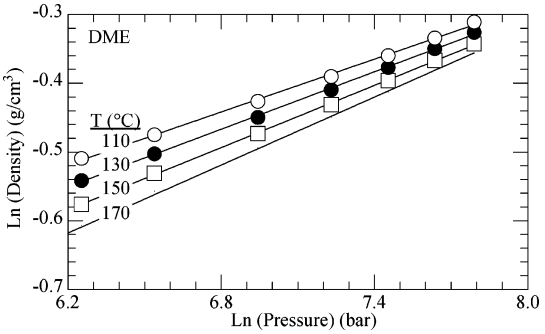

Figure 2. Variation of the density of dimethyl ether (DME) obtained in this study at 110, 130, and 150 °C and pressures to 2400 bar. The curve at 170 °C was extrapolated from the lower temperature curves.

increases by approximately 23% at the operating conditions used in this study, which is 3 times the increase in solvent mass density reported for the scattering studies with PIB−2-methylbutane and PS−butanone systems.[16] The DME density data are subsequently used to analyze the DLS data via estimation of the solvent refractive index and viscosity.

Results and Discussion

Dilute Solution Phase Behavior. The PEB_{10}−DME cloud-point curve shown in Figure 1 exhibits a rapid increase in pressure at temperatures near 105 °C, and in fact, the curve exhibits a positive slope at very high pressures. The type of phase behavior shown in Figure 1 is typical of that found for SCF−polymer mixtures where the SCF solvent is polar and the polymer is nonpolar or vice versa.[41] The existence of both low- and high-pressure UCST branches is readily apparent for temperatures ≥ 105 °C—that is, phase boundaries can be approached twice along a given isotherm. The low-pressure UCST branch is primarily fixed by solvent density, which modulates the strength of polymer−solvent interactions. This low-pressure phase boundary is commonly observed in compressed gas, liquid, and supercritical fluid systems.[41] The inset to Figure 1 indicates that PEB_{10} concentration, in the range used for DLS measurements, has only a minimal effect on the location of the low-pressure UCST. The high-pressure UCST is somewhat more exotic for polymer solutions. Similar behavior has been observed in poly(dimethylsiloxane)−CO_2,[42] perfluorinated poly(isoprene)−CO_2,[43] and perfluorinated poly(butadiene)−CO_2[43] systems as well as some polymer−liquid solvent solutions such as poly(styrene)−deuteriomethylcyclohexane.[18] Lower critical solution temperature and UCST phase boundaries have also been observed at elevated pressures in aqueous polymer systems.[17,44]

Polymer Diffusion in Dilute Solutions. The concentration dependence of the mutual polymer diffusion coefficient, $D(c)$, is commonly expressed as[45]

$$D(c) = D_0(1 + k_D c + ...) \tag{3a}$$

where the second dynamic virial coefficient, k_D, is given by[46]

$$k_D = 2A_2M - k_s \tag{3b}$$

as the authors have previously demonstrated that solution compressibility effects are negligible,[15] thereby indicating that k_D is essentially fixed by the thermodynamic A_2 and hydrodynamic k_s terms retained in eq 3b. k_D, which accounts for polymer−polymer and polymer−solvent interactions, is determined from the slope of $D(c)$ vs c, and the coefficient D_0, the infinite dilution translational diffusion coefficient, is given by the zero concentration intercept.[7] Application of such an analysis requires accurately accounting for pressure-induced changes in the polymer concentration determined from the solution density, which is essentially that of pure solvent for the dilute solutions considered here. The polymer hydrodynamic radius at infinite dilution, R_H, is estimated from the Stokes−Einstein equation $R_H = kT/6\pi\eta D_0$,where η, the solvent viscosity, is estimated, as described previously for the PEB_{10}−alkane mixtures,[15] using the method of Stiel and Thodos.[47]

Dynamic light scattering measurements of polymer diffusion in PEB_{10}−DME solutions are made at pressures ranging from a few bar above the low-pressure UCST up to nearly 2500 bar, thereby ensuring single-phase operation. Figure 3 illustrates the concentration dependence of $D(c)$ for PEB_{10} in DME at 110, 130, 150, and 170 °C for several pressures. Straight line fits of the data suggest that eq 3a can be truncated after the first-order term to obtain reliable k_D values from the slope of the line and D_0 from the zero concentration intercept for each pressure. It is apparent that the infinite dilution translational diffusion coefficients decrease with increasing pressure while the dynamic second virial coefficients increase. Figure 4 shows the variation of D_0 as the system pressure is isothermally increased from the lower pressure phase boundary. The four D_0 curves display similar pressure dependence. As observed in a previous study of PEB_{10}−alkane solutions,[15] the measured diffusivity values are approximately 1 order of magnitude greater than those typically found for a polymer dissolved in a dense liquid solvent even though DME exhibits liquidlike densities ranging from 0.54 to 0.73 g/cm^3 at the investigated pressures. As shown in Figure 5, pressure-induced viscosity changes account for all of the variation observed in the infinite dilution diffusivity at a given temperature. Therefore, the Stokes−Einstein equation suggests R_H is independent of pressure in DME at all the investigated temperatures, as shown in Figure 6. This behavior is analogous to that observed for the polystyrene−toluene system[13−15] where pressure-induced viscosity changes account for essentially the entire corresponding change in D_0. It is also apparent from Figure 6 that the hydrodynamic radii are also independent of temperature. The temperature and pressure independence of the hydrodynamic radii are considered further below. It should be noted that these R_H values are essentially equivalent to the R_g values reported for an earlier SANS investigation[25] of PEB_{10}−dimethyl ether solutions when one would expect that $R_H < R_g$ at the same polymer concentration. Since the previous study considered solution concentrations near the overlap region, not at infinite dilution, it is suspected that some chain contraction has taken place. In fact, the reported SANS R_g values are slightly smaller than the predicted unperturbed R_g for the melt confirming the likelihood of some chain contraction near the overlap region. In addition, both the refractive index and viscosity are estimated by extrapolation into the high-density region. This extrapolation could lead to a systematic error of ±15% in the determined R_H values which would have no qualitative effect on the observed trend in R_H.

As previously mentioned, Figure 3 demonstrates that the concentration dependence of the mutual diffusion

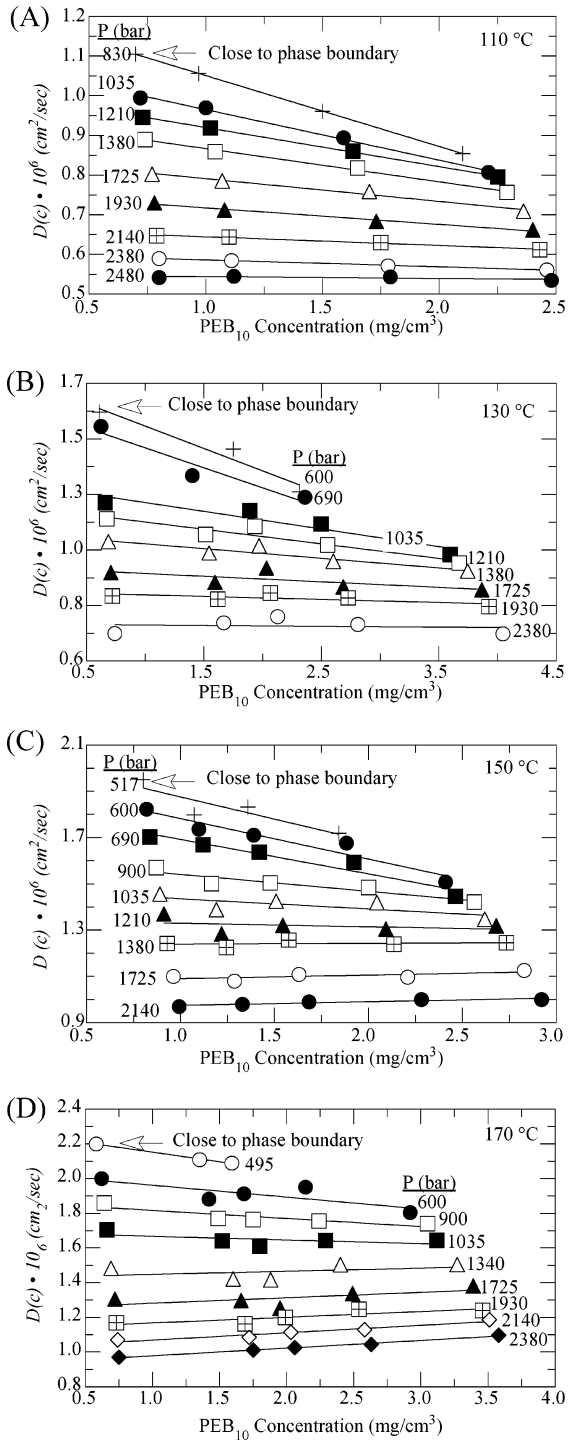

Figure 3. Pressure dependence of the mutual translational diffusion coefficient, $D(c)$, for PEB_{10} in dimethyl ether at 110 (A), 130 (B), 150 (C), and 170 °C (D). In these figures not all of the experimental pressures are shown to avoid cluttering the plot.

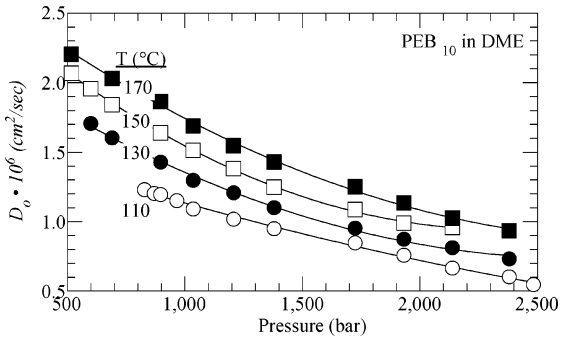

Figure 4. Variation of the infinite dilution polymer translational diffusion coefficient, D_0, as a function of pressure for PEB_{10} in dimethyl ether at 110, 130, 150, and 170 °C. The low-pressure limit of each curve terminates at the low-pressure UCST branch. Note that the high-pressure limit of the 110 °C curve also terminates at the high-pressure UCST branch.

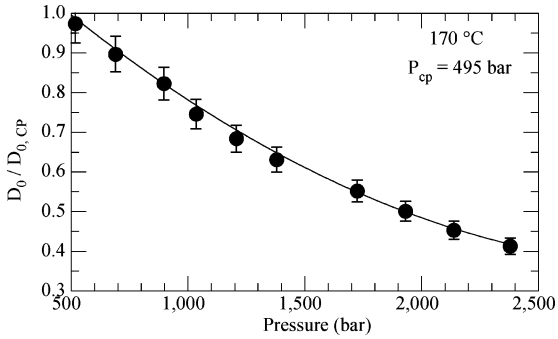

Figure 5. Impact of solvent viscosity, η_{cp}/η (solid line), on the infinite dilution translational diffusion coefficient, $D_0/D_{0,cp}$ (circles), for PEB_{10}−DME solutions at 170 °C. The subscript cp represents the value at the cloud point. The change in solvent viscosity essentially accounts for all the observed diffusivity variation as was also observed for PEB_{10}−DME solutions at 110, 130, and 150 °C. The error bars are representative of the estimated error present in measured diffusion coefficients.

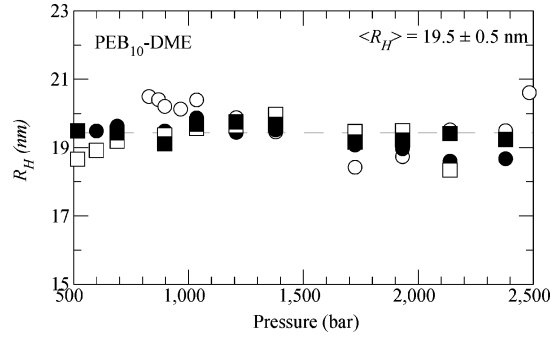

Figure 6. Infinite dilution hydrodynamic radius, R_H, for PEB_{10}−DME mixtures at 110 (○), 130 (●), 150 (□), and 170 °C (■) is essentially independent of pressure and temperature.

coefficient can be reasonably fit with a straight line, suggesting that eq 3a can be truncated after the first-order term to obtain reliable information on k_D from the slope of each isobar. In general, the isobars in Figure 3 exhibit negative slopes upon approach to the low-pressure UCST branch with the slopes becoming less negative as the pressure increases and eventually displaying slightly positive values at the highest pressures considered. Similar pressure-induced changes in the sign of k_D, while operating in the single-phase region and close to a phase boundary, have also been observed for both aqueous PVP[17] and PEB_{10}−alkane solutions.[15] However, the change in the behavior of k_D for the aqueous PVP solutions owes to the reduction of hydrogen bonding between the pyrrolidone group and water with increasing pressure, whereas the change in the behavior of k_D for the PEB_{10}−alkane systems is related to the weakening of van der Waals dispersion-type interactions with decreasing pressure. That is, an increase in monomer−monomer attractive forces occurs as the decreasing solvent density reduces solvent screening of these interactions as predicted by recent computer

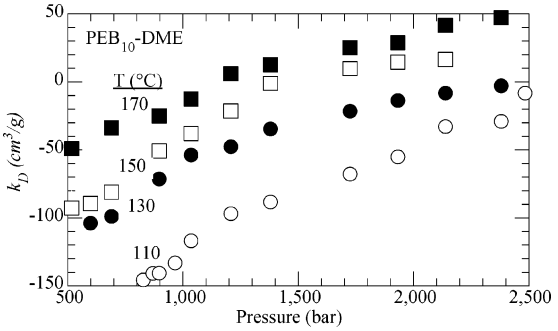

Figure 7. Variation of the dynamic second virial coefficient, k_D, for PEB_{10} dissolved in DME as a function of pressure at 110 (○), 130 (●), 150 (□), and 170 °C (■).

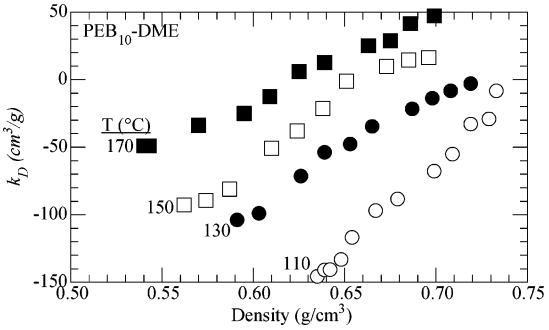

Figure 8. Variation of the dynamic second virial coefficient, k_D, as a function of density for PEB_{10} in DME at 110 (○), 130 (●), 150 (□), and 170 °C (■).

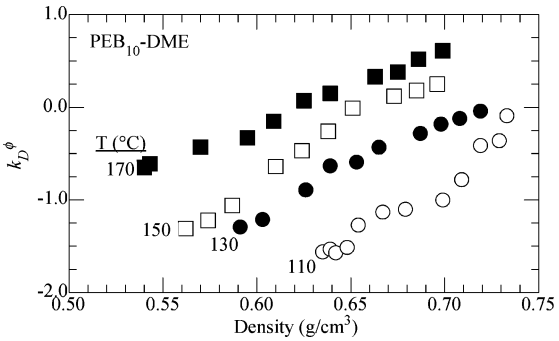

Figure 9. Variation of the volume fraction based dynamic second virial coefficient, k_D^ϕ, as a function of density for PEB_{10} in DME at 110 (○), 130 (●), 150 (□), and 170 °C (■).

simulations.[48−50] In both cases, increasingly unfavorable polymer−solvent interactions near the phase boundary lead to the observed phase separation. Figure 7 shows the variation of k_D as a function of pressure in the single-phase region for the PEB_{10}−DME system. It is apparent that k_D increases with increasing pressure and temperature, indicating that the solvent quality of DME is also increasing. As noted previously, no corresponding increase in hydrodynamic radius is observed with changes in pressure, suggesting that while polymer coils slowly expand they become more free draining. Kermis and co-workers previously reported that k_D for PEB_{10}−alkane solutions at 130 °C only depends on the "methyl" molar density, which is the solvent molar density multiplied by the number of $CH_3 + CH_2$ groups in the solvent.[15] The methyl molar density crudely reflects a measure of the strength of pairwise dispersion interactions[51] between a conveniently chosen segment of each normal alkane and a repeat group of PEB_{10}. This sort of density scaling is expected to fail for the PEB_{10}−DME system due to the strong polar nature of dimethyl ether. Indeed, the k_D curves do not collapse to a single curve when plotted against DME density (see Figure 8). The observed temperature dependence of PEB_{10}−DME interactions is likely a result of temperature-dependent, DME−DME polar interactions[48] that dominate PEB_{10}−PEB_{10} or PEB_{10}−DME interactions.

For comparison with previous related investigations, it is more convenient to consider the polymer volume fraction dependence of the mutual polymer diffusion coefficient

$$D(\phi) = D_0(1 + k_D^\phi \phi + ...) \tag{4a}$$

where

$$k_D^\phi = k_D \frac{M}{N_A V_H} \tag{4b}$$

Here V_H is an equivalent hydrodynamic hard-sphere volume defined by the hydrodynamic radius R_H, M is the polymer molecular weight, and N_A is Avogadro's number. Measured hydrodynamic radii are used to convert the measured k_D to k_D^ϕ as defined in eq 4b, and k_D^ϕ values are presented in Figure 9 as a function of DME density. The k_D^ϕ data are noisier than the k_D values presented in Figures 7 and 8 as a result of the noisy R_H values that enter the k_D^ϕ calculation via the hydrodynamic volume which has a third-order dependence on R_H. The results observed here are consistent with the findings reported by Cotts and Selser[7] for conventional polymer−liquid solvent solutions as well as previous investigations of PEB_{10}−alkane solutions by the current authors.[15] In the present case, DME solvent quality is best classified as marginal since the measured k_D^ϕ values all lie well within the best estimate of the Θ condition ($k_D^\phi = -2$)[7] and the limit expected for good solvents ($k_D^\phi \cong 2$).[7] The relatively weak variation in DME solvent quality with pressure or density is reflected in the essentially constant values of the hydrodynamic radius. Interestingly, unlike the case for PEB_{10}−alkane solutions,[15] sub-Θ solubilization of PEB_{10} in DME is not observed; that is, the low-pressure phase separation of PEB_{10}−DME solutions occurs upon approach to the Θ condition without a rapid decrease in k_D^ϕ and without a concomitant decrease in R_H.

It should be noted that while the highest pressure considered at 110 °C is just a few bar below the high-pressure UCST branch illustrated in Figure 1, there is no concurrent decrease in k_D as the high-pressure UCST is approached. This observation is unlike the behavior observed upon approach to the low-pressure UCST in the present case and to liquid−liquid phase boundaries in other systems where k_D was observed to decrease.[7,15,17] Upon approach to the high-pressure UCST, k_D continually increases and, therefore, A_2 also increases since[7]

$$k_D^\phi \propto A_2/R_H^3 \tag{5}$$

To the authors' knowledge, this is the first time that it has been demonstrated unequivocally that phase separation occurs even in the presence of favorable polymer−solvent interactions. It should be noted that high DME densities lead to enhanced DME−DME polar interactions even though A_2 is slowly increasing. Hence, the observed phase separation must be a result of the

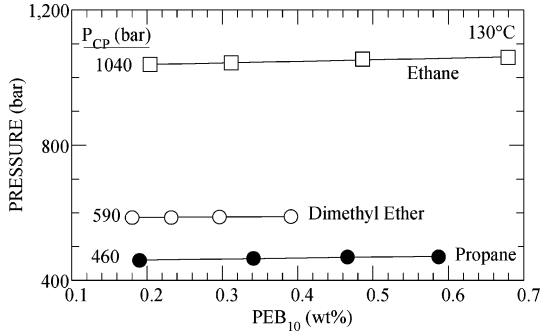

Figure 10. Comparison of the phase behavior of PEB_{10} in ethane,[15] propane,[15] and DME.

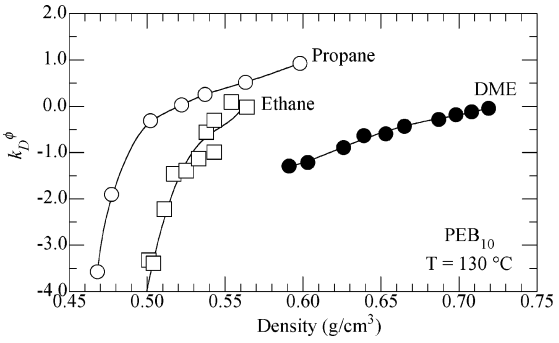

Figure 11. Comparison of the behavior of k_D^{ϕ} for PEB_{10} in ethane,[15] propane,[15] and DME. The pressure range for the DLS measurements are between each respective phase boundary and ~2500 bar.

solution compressibility and not a result of intermolecular interactions since A_2 reflects the monomer excluded volume, **v**, with $A_2 \sim \mathbf{v}$ in the near-Θ region and $A_2 \sim \mathbf{v}^{0.53}$ in the good solvent regime where chains are essentially impenetrable.[1] The high-pressure UCST is most likely caused by an unfavorable excess volume of mixing at high pressures[52−54] wherein PEB_{10} chains cannot be dissolved without perturbing DME from its preferred close-packed, high-density state. That is, PEB_{10} dissolution would generate unfavorable free volume which would increase the free energy of the *system* that leads to phase separation on entropic grounds.

The macroscopic phase behavior at 130 °C in Figure 10 shows that DME is a much better solvent than ethane, but not as good a solvent as propane on a pressure basis. Very high pressures are required with ethane to increase its density to compensate for ethane's intrinsically weak interaction strength. Conversely, polar DME has less favorable polymer−solvent interactions than nonpolar propane, which means that DME densities in excess of those needed with propane are required to improve DME solvent quality. Figure 11 shows explicitly that DME solvent quality, as manifested in k_D^{ϕ}, increases only very slowly with increasing mass density as compared to the solvent quality of both ethane and propane. Although propane and DME exhibit similar rates of increase in k_D^{ϕ} with high pressures (i.e., at the highest respective densities), the lower absolute value of k_D^{ϕ} observed for DME is the result of less favorable nonpolar PEB_{10}−polar DME interactions that become magnified at high densities. These observations are consistent with an expected more rapid increase of A_2 near the Θ condition and then a decreasing rate of A_2 increase in the swollen chain region as mentioned previously. A linear extrapolation of the high-pressure branch of the PEB_{10}−DME UCST suggests that this solution would phase separate at approximately 4500 bar at 130 °C, which corresponds to a DME density of ~0.78 g/cm^3 or 0.017 mol/cm^3. Unfortunately, the DME data were obtained to densities of only ~0.74 g/cm^3 (0.016 mol/cm^3), and this branch of the UCST was not observed at 130 °C. In contrast, at pressures close to 2500 bar, the mass density of propane is ~0.60 g/cm^3 (0.014 mol/cm^3), which is less than that of DME. Since these molecules are relatively similar in both size and shape, this density difference reflects the ability of polar DME to "self-associate" in a more ordered manner than propane. This enhanced solvent packing is expected to increase with increasing pressure and decreasing temperature. In comparison with DME, nonpolar propane evidently packs more effectively around and within a PEB_{10} coil without severely compromising its preferred packing density, thus promoting a favorable entropy of mixing. While a direct comparison between ethane and DME is problematic because of size differences, it is conjectured that ethane can also pack effectively around and within a PEB_{10} coil.

Conclusions

The high-pressure DLS investigation described here provides insight into the response of nonpolar PEB_{10} chains to a wide variation in the chemical potential environment provided by polar dimethyl ether. The macroscopic phase behavior for the PEB_{10}−dimethyl ether displays both low- and high-pressure upper consolute temperature branches. The DLS data show that the polymer translational diffusion coefficient at infinite dilution, D_0, increases with increasing temperature at all pressures, as expected. However, the variation of D_0 with pressure along a given isotherm is inversely proportional with solvent viscosity, indicating that the hydrodynamic radii of PEB_{10} chains dissolved in dimethyl ether are independent of pressure. In fact, the hydrodynamic radii are independent of both temperature and pressure for this system.

At all temperatures, k_D, which represents a balance between thermodynamic interactions and hydrodynamic forces, starts at low negative values at conditions near the low-pressure UCST and increases with increasing pressure until eventually becoming positive in some cases. However, the observed k_D^{ϕ} values are between the values expected for Θ and good solvents. In fact, it appears that dimethyl ether is just a marginal solvent for PEB_{10} even at very high pressures. This is consistent with the observation that the hydrodynamic radii, at all conditions, remain essentially constant, reflecting the small increases in chain expansion counterbalanced by the small increases in chain draining. The decrease of k_D upon approaching the low-pressure UCST is consistent with the expected weak polymer−solvent interactions at such low densities. More interesting is the observation that k_D continues to increase as the high-pressure UCST is approached, thereby indicating that this phase boundary is entropic in origin. The most likely explanation is unfavorable mixing effects owing to the failure of PEB_{10} to successfully pack into the dense dimethyl ether. To the authors' best knowledge, this is the first experimental confirmation of the entropic origin of the high-pressure UCST behavior observed in a polymer solution.

Acknowledgment. M.A.M. and J.v.Z. acknowledge the National Science Foundation (NSF) for partial support of this project under Grant CTS-9729720. Acknowledgment is made by M.A.M. to the donors of the American Chemical Society Petroleum Research Fund for partial support of this research. Special acknowledgment is given to Dr. Pamela Wright and Dr. Lewis Fetters for providing the high-quality PEB_{10} used in these studies.

References and Notes

(1) Rubinstein, M.; Colby, R. H. *Polymer Physics*; Oxford University Press: Oxford, 2003.
(2) Berne, B. J.; Pecora, R. *Dynamic Light Scattering*; Dover Publications: Mineola, NY, 2000.
(3) Cummins, H. Z.; Pike, E. R. *Photon Correlation and Light Beating Spectroscopy*; Plenum Press: New York, 1973.
(4) Akcusa, A. Z.; Benmouna, M. *Macromolecules* **1978**, *11*, 1193.
(5) Han, C. C.; Akcusa, A. Z. *Polymer* **1981**, *22*, 1165.
(6) Akcusa, A. Z. *Polymer* **1981**, *22*, 1169.
(7) Cotts, P. M.; Selser, J. C. *Macromolecules* **1990**, *23*, 2050−2057.
(8) Lechner, M. D.; Schulz, G. V. *J. Colloid Interface Sci.* **1972**, *39*, 469−471.
(9) Lechner, M. D.; Schulz, G. V.; Wolf, B. A. *J. Colloid Interface Sci.* **1972**, *39*, 462−468.
(10) Lechner, M. D. *Ber. Bunsen-Ges.* **1977**, *10*, 992−995.
(11) Jeremic, K.; Ilic, L.; Jovanovic, S.; Lechner, M. D. *Eur. Polym. J.* **1989**, *25*, 281−284.
(12) Stankovic, R. I.; Jovanovic, S.; Ilic, L.; Nordmeier, E.; Lechner, M. D. *Polymer* **1991**, *32*, 235−240.
(13) Roots, J.; Nystrom, B. *Macromolecules* **1982**, *15*, 553−556.
(14) Freeman, B. D.; Soane, D. S.; Denn, M. M. *Macromolecules* **1990**, *23*, 245−251.
(15) Kermis, T. W.; Li, D.; Guney-Altay, O.; Park, I. H.; van Zanten, J. H.; McHugh, M. A. *Macromolecules* **2004**, *37*, 9123−9131.
(16) Gaeckle, D.; Patterson, D. *Macromolecules* **1972**, *5*, 136−141.
(17) Sun, T.; King Jr., H. E. *Phys. Rev. E* **1996**, *54*, 2696−2703.
(18) Szydlowski, J.; Rebelo, L. P. N.; Wilczura, H.; Dadmun, M.; Melnichenko, Y. B.; Wignall, G. D.; van Hook, W. A. *Phys. B* **1998**, *241−243*, 1035−1037.
(19) Szydlowski, J.; van Hook, W. A. *Macromolecules* **1998**, *31*, 3266−3274.
(20) Szydlowski, J.; van Hook, W. A. *Macromolecules* **1998**, *31*, 3255−3265.
(21) Szydlowski, J.; Rebelo, L. P. N.; Wilczura, H.; Dadmun, M.; Melnichenko, Y. B.; Wignall, G. D.; van Hook, W. A. *Fluid Phase Equilib.* **1998**, *150−151*, 687−694.
(22) van Hook, W. A.; Wilczura, H.; Imre, A.; Rebelo, L. P. N.; Melnichenko, Y. B. *Macromolecules* **1999**, *32*, 7312−7318.
(23) Van Hook, W. A.; Wilczura, H.; Rebelo, L. P. N. *Macromolecules* **1999**, *32*, 7299−7311.
(24) Moses, C. L.; van Hook, W. A. *J. Polym. Sci., Part B: Polym. Phys.* **2003**, *41*, 3070−3076.
(25) DiNoia, T. P.; van Zanten, J. H.; Kline, S. R.; Garach-Domech, A.; McHugh, M. A.; Wright, P. J.; Fetters, L. J. *Macromolecules* **2003**, *36*, 7372−7378.
(26) Rachapudy, H.; Smith, G. G.; Raju, V. R.; Graessley, W. W. *J. Polym. Sci., Part B: Polym. Phys.* **1979**, *17*, 1211−1222.
(27) Kirgas, T. M.; Carella, J. M.; Struglinski, M. J.; Crist, B.; Graessley, W. W. *J. Polym. Sci., Part B: Polym. Phys.* **1985**, *23*, 509.
(28) Balsara, N. P.; Fetters, L. J.; Hadjichristidis, N.; Lohse, D. J.; Han, C. C.; Graessley, W. W.; Krishnamoorti, R. *Macromolecules* **1992**, *25*, 6137−6147.
(29) Fetters, L. J.; Graessley, W. W.; Krishnamoorti, R.; Lohse, D. J. *Macromolecules* **1997**, *30*, 4973−4977.
(30) Provenecher, S. W. *Comput. Phys. Comm.* **1982**, *27*, 213−227.
(31) Provenecher, S. W. *Comput. Phys. Comm.* **1982**, *27*, 229−242.
(32) Hadrich, J. *Appl. Phys.* **1975**, *7*, 209−213.
(33) Vedam, K.; Limsuwan, P. *J. Chem. Phys.* **1978**, *69*, 4772−4778.
(34) Achtermann, H. J.; Magnus, G.; Bose, T. K. *J. Chem. Phys.* **1991**, *94*, 5669−5684.
(35) Conway, S. E. Ph.D. in Chemical Engineering, Johns Hopkins University, Baltimore, MD, 2001.
(36) Johnson, B. L.; Smith, J. In *Light Scattering from Polymer Solutions*; Huglin, M. B., Ed.; Academic Press: New York, 1972; pp 27−39.
(37) Born, M.; Wolf, E. *Principles of Optics: Electromagnetic theory of propagation, interference and diffraction of light*, 7th ed.; Cambridge University Press: New York, 1999.
(38) Diguet, R.; Deul, R.; Franck, E. U. *Ber. Bunsen-Ges. Phys. Chem.* **1985**, *89*, 800−804.
(39) Sen, Y. L.; Kiran, E. *J. Supercrit. Fluids* **1990**, *3*, 91−99.
(40) Byun, H. S.; DiNoia, T. P.; McHugh, M. A. *J. Chem. Eng. Data* **2000**, *45*, 810−814.
(41) Kirby, C. F.; McHugh, M. A. *Chem. Rev.* **1999**, *99*, 565−602.
(42) Melnichenko, Y. B.; Kiran, E.; Wignall, G. D.; Heath, K. D.; Salaniwal, S.; Cochran, H. D.; Stamm, M. *Macromolecules* **1999**, *32*, 5344.
(43) McHugh, M. A.; Park, I. H.; Ren, Y.; Reisinger, J. J.; Lodge, T. P.; Hillmyer, M. A. *Macromolecules* **2002**, *35*, 4653−4657.
(44) Sun, T.; King Jr., H. E. *Macromolecules* **1998**, *31*, 6383.
(45) Vink, H. *Faraday Trans.* **1985**, *81*, 1725.
(46) Tsunashima, Y.; Hashimoto, T.; Nakano, T. *Macromolecules* **1996**, *29*, 3475−3484.
(47) Stiel, L. I.; Thodos, G. *AIChE J.* **1964**, *10*, 275−277.
(48) Luna-Barcenas, G.; Gromov, D. G.; Meredith, J. C.; Sanchez, I. C.; de Pablo, J. J.; Johnston, K. P. *Chem. Phys. Lett.* **1997**, *278*, 302.
(49) Luna-Barcenas, G.; Meredith, J. C.; Sanchez, I. C.; Johnston, K. P.; Gromov, D. G.; de Pablo, J. J. *J. Chem. Phys.* **1997**, *107*, 10782.
(50) Gromov, D. G.; de Pablo, J. J. *Fluid Phase Equilib.* **1998**, *150*, 657.
(51) Prausnitz, J. M.; Lichtenthaler, R. N.; de Azevedo, E. G. *Molecular Thermodynamics of Fluid-Phase Equilibria*, 3rd ed.; Prentice Hall: Englewood Cliffs, NJ, 1999.
(52) Prigogine, I.; Defay, R.; Everett, D. H. *Chemical Thermodynamics*; Longmans Green and Co.: London, 1954.
(53) Patterson, D. *Macromolecules* **1969**, *2*, 672−677.
(54) Rowlinson, J. S.; Swinton, F. L. *Liquids and Liquid Mixtures*, 3rd ed.; Butterworth: London, 1982.

MA048166Y